Journal of Materials Chemistry C

ARTICLE

Domain evolution of tetragonal Pb(Zr$_x$Ti$_{1-x}$) O$_3$ piezoelectric thin films on SrTiO$_3$ (100) surfaces: combined effects of misfit strain and Zr/Ti ratio

Qi Yu,[a] Jing-Feng Li,[*a] Fang-Yuan Zhu,[a] and Jiangyu Li[b]

A series of sol-gel-processed Pb(Zr$_x$Ti$_{1-x}$)$_{0.98}$Nb$_{0.02}$O$_3$ (x=0.2, 0.3, 0.4, 0.52) piezoelectric films were epitaxially grown on (100) surfaces of Nb-doped SrTiO$_3$ single-crystalline substrates to study the composition-dependent domain evolution and corresponding piezoelectricity. The transformation between the 90° *a* and *c* domains throughout the tetragonal phase region, together with the variation of piezoelectric property under different excitation signals, were investigated by piezoresponse force microscopy. The observed domain evolution has been well explained by the combined effects of both misfit strain and tetragonality depending on the Zr/Ti ratio.

1 Introduction

Ferroelectric domain is an important topic in piezoelectric materials.[1-3] Domain configuration and kinetics, especially the non-180° domain wall motion, are closely associated with the overall piezoresponse.[4-6] Compared to bulk materials, thin films are subjected to substantial stress due to the misfit strain between the films and the substrates,[7-11] in which domain wall motion is pinned and suppressed heavily by the existence of stress field. So far, a considerable amount of studies have been carried out on thin films in lead zirconate titanate [Pb(Zr$_x$Ti$_{1-x}$)O$_3$, abbreviated as PZT] system because of their excellent piezoelectric and ferroelectric properties.[12,13] For the tetragonal PZT-based films, the 90° domains associated with the alternating tetragonal *c* domains and the pseudo-tetragonal *a* domains are regarded as a key factor for its outstanding piezoesponse.[14,15] Its configuration and evolution can be affected by the misfit strain especially in the strongly-constraint epitaxial films. Although a few works have already been devoted to this matter,[16-18] more studies are needed to establish the correlations between microscopic domain structure and macroscopic piezoelectric response, especially the *in-situ* observation of domains arrangement in tetragonal PZT-based epitaxial films, and the corresponding measurement of local piezoelectric property under modulated electrical fields.

In this work, a series of <100>-oriented Pb(Zr$_x$Ti$_{1-x}$)$_{0.98}$Nb$_{0.02}$O$_3$ epitaxial films (PNZT) with a wide range of composition were deposited onto 1% Nb-doped [100]-cut SrTiO$_3$ single-crystalline substrates (abbreviated as Nb:STO) using the sol-gel approach. The <100> orientation was thought to be advantageous in terms of piezoelectric anisotropy, and its relatively simple domain structure is amenable for deeper investigation.[19] The Nb dopant in PZT films can promote electrical properties,[20-22] whereas it enhances conductivity of the STO substrates without changing the intrinsic phase structure.[23] To probe local piezoelectricity non-destructively, surface piezoresponse together with domain mapping were obtained by using piezoresponse force microscopy (PFM).[24,25] Domain transformation was then explained by the combined effects of both compressive misfit strain and tetragonality among various Zr/Ti ratios.

2 Experimental

Synthesis

Sol-gel approach was employed for the preparation of PNZT epitaxial thin films. Trihydrate lead acetate [Pb(CH$_3$COO)$_2$•3H$_2$O] was dissolved in 2-methoxyethanol (2-MOE) and refluxed. Then zirconium n-propoxide [Zr(OCH(CH$_3$)$_2$)$_4$], titanium isopropoxide [Ti(OCH(CH$_3$)$_2$)$_4$], and niobium ethoxide [Nb(OC$_2$H$_5$)$_5$] were added into the precursor solution as raw materials together with 2-methoxyethanol, acetylacetone, and methanamide as solvent, chelating agent, and stabilizing agent, respectively. A total of 10 mol% excess Pb was introduced into all solutions with different Zr/Ti ratios to compensate for Pb loss owing to the oxidation and volatilization during the subsequent thermal processing. The precursor solutions were aged and deposited onto (100) surfaces of single-crystalline Nb:STO substrates

This journal is © The Royal Society of Chemistry 2013

J. Mater. Chem. C, 2013, **00**, 1-3 | 1

[Nb:STO(100)] by repeating spin-coating, followed by thermal treatments for pyrolysis and crystallization annealing. The detailed parameters have been already reported elsewhere.[23]

Characterization

The crystallographic structure of the PNZT thin films was examined by X-ray diffraction (XRD, D/max-2500 and D/max-RB, Rigaku; Tokyo, Japan) using Cu-Kα radiation. Typical Phi-scan XRD patterns were obtained by collecting the (111) reflections. The cross-sectional morphology and lattice matching were observed using a transmission electron microscope (TEM, F20, Tecnai; Hillsboro, Oregon). Surface morphology and domain configuration of PNZT films were investigated using PFM (MFP-3D, Asylum Research; CA, USA). An AC excitation signal was applied to the Pt-coated silicon tips with the Nb:STO substrates as counter electrodes, whereas an additional sequence of DC voltage was used for the local ferroelectric measurement. Details of PFM measurements are described elsewhere together with the dual frequency resonance tracking techniques (DFRT), which amplifies the piezoresponse signals by exciting and tracking the resonance frequency of the tip/film surface system.[26,27] The 100-nm-thick Pt round electrode with a diameter of 0.3 mm was sputtered onto samples surface though a metal mask. The film was thus sandwiched by the Pt top electrode and the Nb:STO bottom electrodes so that the ferroelectric test could be carried out and presented as a polarization (P_r) versus electrical field (E_c) plot.
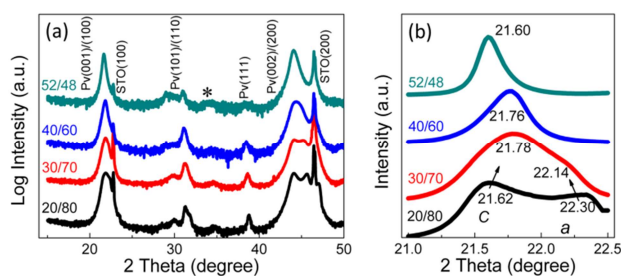
Fig. 1 (a) XRD full patterns of the PNZT films on (100) surfaces of Nb-doped $SrTiO_3$ substrates with various Zr/Ti ratios, (b) step-scanning patterns.

3 Results and Discussion

Microstructure and morphology

XRD full patterns of various PNZT films on Nb:STO(100) are displayed in Fig. 1a with the intensity shown in logarithmical scale. All the films ranging from Zr/Ti=20/80 to 52/48 are found to be pure perovskite phase without any secondary phases within the detect limit of XRD. Diffraction peaks could be indexed as a tetragonal structure by considering the obvious splitting or broadening of the (001)/(100) and (002)/(200) signals. Our previous studies also confirmed that the selected compositions from Zr/Ti=20/80 to 52/48 belong to the tetragonal phase.[28,29] Despite the presence of some weak peaks corresponding to (101)/(110) and (111) planes, the remarkable (100)/(001) preferred orientation was observed for all the

samples. The minor signal at ~33° (marked "*") appears occasionally under logarithmic scale, which should be ascribed to the tiny imperfections or random interface defects in the commercial STO single-crystalline substrates. In order to clarify the phase structure more accurately, the step-scanning method was employed to measure the (100)/(001) peaks, and the results are shown in Fig. 1b. According to a previous study, the intensities of (100) and (001) peaks can be associated with the pseudo-tetragonal *a* domains and the alternating tetragonal *c* domains in tetragonal PZT-based system, respectively.[30] It can be seen obviously that the (100)/(001) peak splitting disappears gradually with the increasing Zr/Ti ratio, indicating the decreased tetragonality (*c/a* ratio) of PNZT unit cell. The XRD results show that the *a* and *c* domains coexist in a great extent at Zr/Ti=20/80, then the signals of *a* and *c* domains move closer at Zr/Ti=30/70, which signifies the expanded *a* axis and the contracted *c* axis in PNZT unit cell.[28] Meanwhile, the relative intensity of *c* domains at the lower angle side appears to be stronger than that of *a* domains at the higher angle side, suggesting that more *c* domains appear at Zr/Ti=30/70 than those at 20/80. The narrower single peak corresponding to *c* domains can be observed when the Zr/Ti ratio is increased to 40/60 and 52/48. The (001) peak moves towards the lower angle side at Zr/Ti=52/48 than that of 40/60, which indicates the out-of-plane *c* parameter starts to expand slightly at certain Zr/Ti ratio after initial shrinking.[28] Moreover, peaks for *a* domains all appear at the lower angle side to the corresponding STO peaks in Fig. 1, which reveals a larger lattice parameter along the in-plane direction in films than that of STO. So films should bear compressive strain in terms of in-plane mismatching.
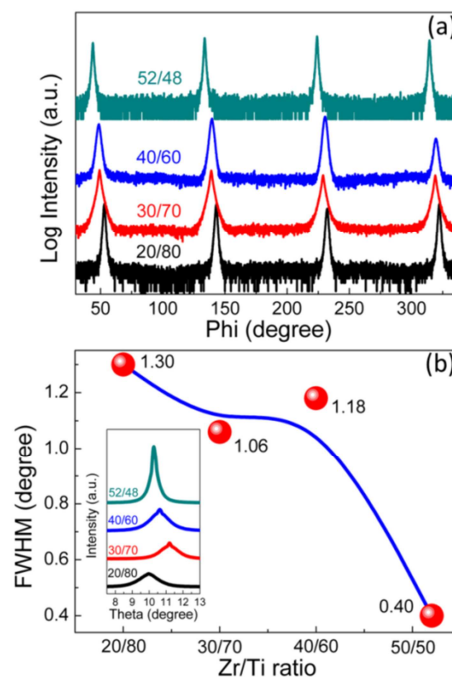
Fig. 2 (a) Phi-scan profiles, (b) rocking curve collections of PNZT epitaxial films with corresponding FWHM values.

2 | *J. Mater. Chem. C*, 2013, **00**, 1-3

This journal is © The Royal Society of Chemistry 2012

To confirm the epitaxial growth in film system, Fig. 2a depicts the Phi-scans of all the PNZT samples. The Phi-scans show the four-fold tetragonal symmetry with 90° intervals, suggesting a well-structured in-plane ordering inheriting from the cubic Nb:STO(100) substrate.[30] The variation of the FWHM (Full Width at Half Maximum) values of PNZT (100) peaks is presented in Fig. 2b as a function of Zr/Ti ratios. Compared to values reported previously in the epitaxial films,[31,32] our FWHM level throughout the selected compositions indicates a well-crystallized state. The relatively large values at Ti-rich region can be ascribed to the broadening (001)/(100) splitting. A sharp decline appears when the composition moves to Zr/Ti=52/48, indicating a weakening trend of the coexistence of a and c domains.
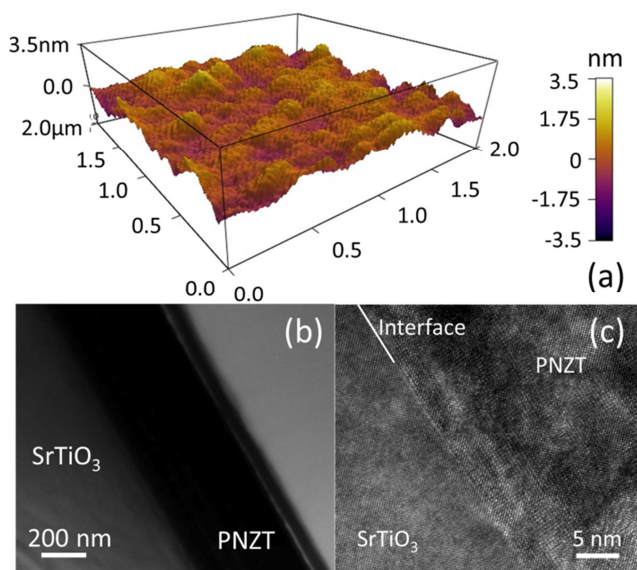
Fig. 3 (a) Surface morphology of PNZT films on Nb:STO(100) substrates, (b) TEM cross-sectional image of PNZT film, (c) high-resolution image of interface between film and substrate.

Surface morphology was investigated using PFM under contact mode within a square area of 2 μm^2, as shown in Fig. 3a. A smooth surface free of cracks or defects was obtained with a small surface roughness value (RMS=0.51 nm). The cross-sectional TEM image shown in Fig. 3b reveals that the PNZT film has a uniform thickness of about 350 nm. As shown in Fig. 3c, high-resolution microscopy at the interface region between film and Nb:STO substrate illustrates the clear epitaxial relationship with rigid lattice matching. The interplanar spacing in PNZT films (0.412 nm) is larger than that of Nb:STO substrates (0.399 nm), confirming that the film layer is subjected to compressive strain to keep the epitaxy with the STO substrates.[29]

Domains and electrical property

Surface vibration detected by PFM tips is expected to yield piezoelectric amplitude and phase information, thus revealing structural details of ferroelectric domains. By applying a small

sinusoidal AC voltage of 5 V through the PFM tip in contact with film surface, the out-of-plane (OP) piezoelectric amplitudes and phases of films with compositions ranging from Zr/Ti=20/80 to 52/48 were obtained within a square area of 2 μm^2 (Fig. 4).

For the Zr/Ti=20/80 film, the OP amplitude mapping exhibits considerably contrast as the evidence of the coexisting a and c domains. The areas with a relatively large response value (yellow regions) correspond to the out-of-plane c domains, whereas the other parts with low amplitude (blue regions) are likely to be the in-plane a domains. The large difference of phase value symbolizes different polarization directions at vertical dimension. When the composition moves to Zr/Ti=30/70, the a and c domains continue to coexist with finer size from the amplitude mapping. An obvious deviation takes place in the case of Zr/Ti=40/60, where amplitude and phase mappings show homogeneous configuration with no notable contrast. This can be interpreted as the dominant role of c domains in films, also consistent with our XRD results. There is no obvious phase discrepancy corresponding to the upward and downward c domains, which may be ascribed to the inner bias in PZT-based system thereby facilitating the polarization behavior along one preferred direction.[33] As a whole, the OP amplitude value corresponding to c domains (yellow regions in Zr/Ti=20/80, 30/70 and almost the entire area in 40/60) are comparable with one another in all the three compositions, the reason would be explained later. When the Zr/Ti ratio is increased to 52/48, the films show a remarkable dropping of the OP amplitude, and both the amplitude and phase mappings manifest no contrast, corresponding to a homogeneous domain configuration with limited piezoelectric property.

In order to characterize piezoelectric property among various compositions of PNZT thin films, a pre-designed DC voltage profile ranging from +30V to -30V (for Zr/Ti=20/80 composition, the voltage was elevated to 50V to obtain complete response curve) was applied onto the film samples with an increment of 1V.[34] To avoid structural complexity when multiple domains are involved, the DC begins with the negative maximum voltage of -30V (-50V in 20/80 composition) to pole the sample. During the interval of step-varying DC voltage, a modulated AC voltage of 2V was applied to excite surface piezoresponse with DFRT techniques.[26] Typical butterfly-shaped piezoresponse loops for different Zr/Ti ratios are plotted in Fig. 5a, together with their corresponding piezoresponse hysteresis loops, as shown in Fig. 5b.

Compared to the piezoresponse measured in Fig. 4 in the absence of DC voltage, here we focus on the piezoelectric amplitude at maximum voltage, representing a single c domain state at local region probed by PFM. For Zr/Ti=20/80 composition, the amplitude seems to be limited with obvious asymmetric characteristics. The phase hysteresis of Zr/Ti=20/80 also manifests asymmetric behavior with a considerably large coercive field, which should be related to the additional work to rotate a domains to c domains in this composition with large c/a ratio.[5] Piezoelectric amplitudes after poling increases rapidly with decreasing coercive field when

This journal is © The Royal Society of Chemistry 2012

J. Mater. Chem. C, 2013, **00**, 1-3 | **3**
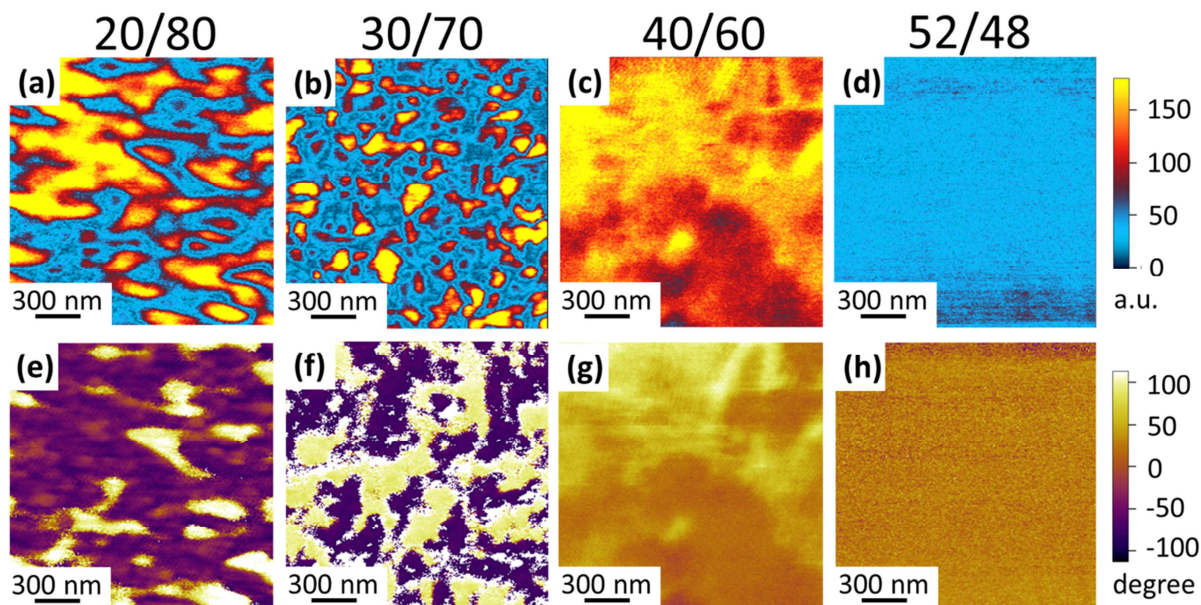
Fig. 4 Piezoresponse mappings of (100)/(001)-oriented PNZT epitaxial films, including (a)-(d) amplitude and (e)-(h) phase collections for different Zr/Ti ratios of 20/80, 30/70,40/60 and 52/48, respectively.

the Zr content is increased to 0.3 and 0.4. With further increasing Zr/Ti ratio to 52/48, the piezoresponse subsequently decreases sharply, and the reason will be discussed below. After obtaining the typical loops at local areas, the piezoresponse test was performed repeatedly within a 2×2-μm-sized mesh of 256 points for all the Zr/Ti ratios to ensure the reliability of our piezoelectric comparison.[19] Ten curves with largest voltage-induced displacement were selected to calculate the average displacement values at the negative maximum voltage as a quantitative parameter. Average values of 151.8, 384.8, 483.5 and 144.8 (a.u.) are obtained for Zr/Ti=20/80, 30/70, 40/60 and 52/48, respectively, consistent with the above piezoresponse variation.

An electrical field was then applied onto PNZT films to detect ferroelectric responses with an excitation frequency of 100 Hz at room temperature. Representative ferroelectric hysteresis loops with the four different Zr/Ti ratios were plotted in Fig. 6. All the films show complete response loops with high polarization values, indicating their excellent ferroelectric property. The giant coercive field values (E_c) should be ascribed to the severe constraint effect from single-crystalline substrates with the limited film thickness.[15] For the Zr/Ti=20/80 composition, the loop manifests a considerably large coercive field with an obvious asymmetric characteristic along the E-axis, similar with the piezoresponse test result shown in Fig. 5b. The Zr/Ti=20/80 film also possesses a relatively small remnant polarization value (P_r) than the Zr/Ti=30/70 and 40/60 ones. This can be ascribed to the multiple in-plane a domains, which may be hard to be rotated to c domains completely even though under a large external excitation. Then the E_c value of PNZT films shows a continuously decreasing trend with increasing Zr/Ti ratio, while the remnant polarization value (P_r) increases

at Zr/Ti=30/70 and 40/60 compositions. The ferroelectric response drops remarkably at Zr/Ti=52/48, consistent with previous piezoelectric property measurement in Fig. 5a.
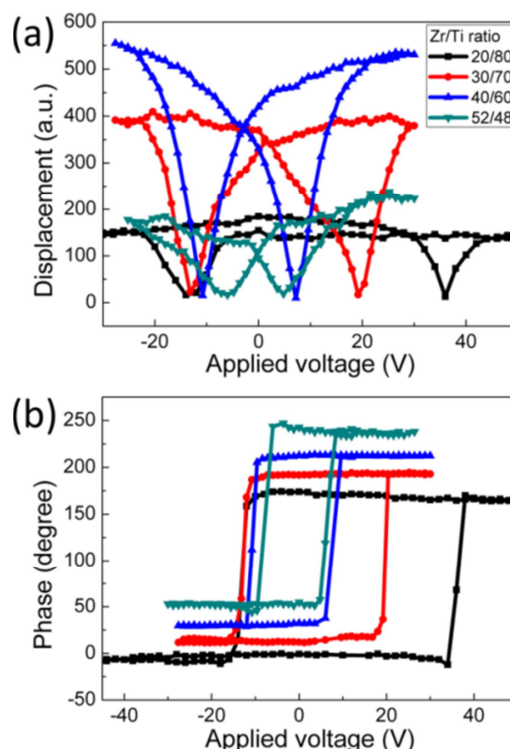
Fig. 5 Piezoelectric response under electrical poling of the PNZT films with various Zr/Ti ratios. (a) typical amplitude-voltage curves, (b) piezoresponse hysteresis loops.
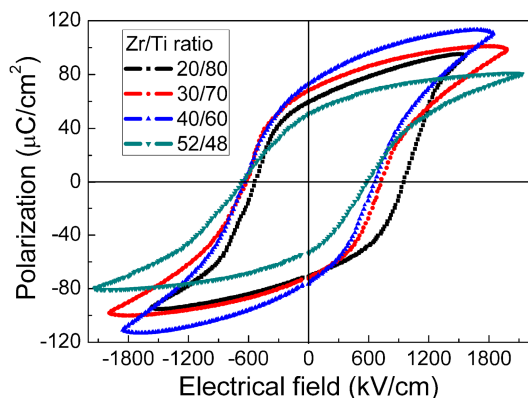
Fig. 6 Typical ferroelectric hysteresis loops of (100)/(001)-oriented PNZT epitaxial films with various Zr/Ti ratios.

Discussion of domain evolution

To clarify the combined effects of misfit strain and Zr/Ti ratio on domain evolution as well as piezoelectric property, a phenomenological mechanism for the tetragonal phase region is established, as schematically depicted in Fig. 7. For the composition range considered, the in-plane *a* parameter of a PNZT unit cell expands continuously from Zr/Ti =20/80 to 52/48, which brings about two coupling aspects. On one hand, with increasing Zr/Ti ratio, the tetragonality would decrease with a reduced *c/a* ratio,[28,35] which has negative effect on the displacement polarization of central Zr/Ti atoms. On the other hand, the expanding in-plane lattice parameter would increase the misfit degree to the Nb:STO substrates. The compressive strain would become more severe with the composition moving to the Zr-rich side. This can in turn promote the conversion of *a* domains into *c* domains, enhancing the displacement polarization in *c* domains.[36]

Domain mappings together with the corresponding piezoresponse before and after poling reflect these coupling factors. When the composition is Zr/Ti=20/80, the coexistence of *a* and *c* domains is obvious under a small voltage excitation, which shows two types of piezoresponse region along vertical direction. This configuration can be also confirmed by related literatures theoretically and experimentally.[17,37] For this composition, the compressive strain is smaller compared to Zr/Ti=30/70 and 40/60 ones due to a relatively small in-plane *a* parameter, and thus the constraint effect would be weak and the extrinsic piezoresponse originating from domain wall motion under small voltage may not be neglected. Then the *a* domains would be rotated to the out-of-plane *c* domains under the large external DC voltage with a large coercive field. After saturated poling, the extrinsic contribution at local areas would be limited, leading to the obvious decreasing of piezoresponse under large DC voltage compared to the two other compositions. When increasing the Zr content to 30/70, the *a/c* coexistence still emerges with a finer size in the PFM mapping. Under DC voltage, the 90° domain rotation can happen easier due to the limited tetragonality and a finer domain size, which brings about a smaller coercive field (Fig. 5b). Then the *c* domains are becoming dominant with few in-plane *a* domains in

Zr/Ti=40/60 composition, giving rise to homogeneous PFM mapping outputs with the increasing piezoresponse and decreasing coercive field after poling.[38] In addition, tetragonality of Zr/Ti=40/60 (so as in 30/70) is much smaller than that of 20/80 one, thus weakening the displacement polarization of central Zr/Ti atoms. However, an increasing of in-plane lattice parameter would increase the compressive misfit strain, which counters the reduction in polarization. By cancelling out these two factors, the OP amplitude of *c* domains in Zr/Ti=40/60 sample is still comparable with that of Zr/Ti=30/70 and 20/80, as mentioned before. The absolute single *c* domain state should finally take place at Zr/Ti=52/48.[28,39] The films would show a pseudo-cubic structure with a much lower *c/a* ratio, which can be the reason for an abrupt decline of piezoelectric property along *c*-axis measured in Fig. 5a.
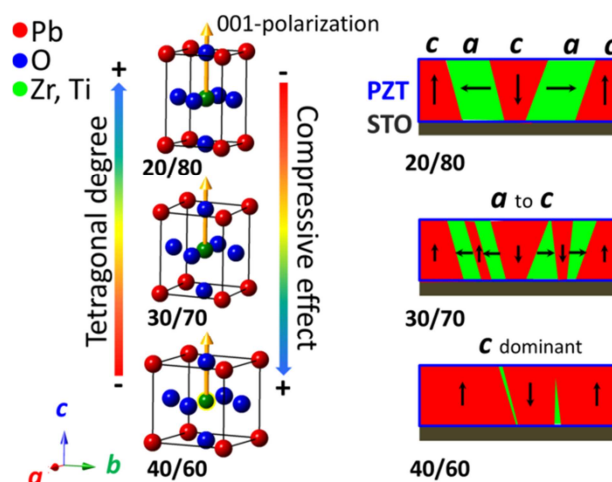
Fig. 7 Schematic illustration of domain evolution in PNZT thin films throughout tetragonal phase area, where the effects of the compressive strain and the composition-dependent tetragonality are highly-coupled.

Conclusions

A collection of PNZT films epitaxially deposited on the (100) surfaces of Nb:STO single-crystalline substrates was studied with an emphasis on *in-situ* domain observation and the corresponding piezoelectric property measurement. By analyzing the combined effects of both the compressive misfit strain and the composition-dependent tetragonality, a phenomenological mechanism was proposed to describe the 90° *a/c* domain configuration and transformation throughout the tetragonal phase region. The present work revealed subtle correlations among domain structure, its evolution, as well as electrical performance under epitaxial strain field, which shed further insight into domain engineering of piezoceramics under constraint conditions.

Acknowledgements

Notes and references

aState Key Laboratory of New Ceramics and Fine Processing, School of Materials Science and Engineering, Tsinghua University, Beijing, 100084, China. E-mail: jingfeng@mail.tsinghua.edu.cn; Fax: +86-62771160; Tel: +86-10-62784845.

bDepartment of Mechanical Engineering, University of Washington, Seattle, Washington 98195-2600, USA. E-mail: jjli@u.washington.edu; Fax: 206-685-8047; Tel: 206-543-6226.

1   C.-L. Jia, K. W. Urban, M. Alexe, D. Hesse and I. Vrejoiu, *Science.*, 2011, **331**, 1420.

2   S. Buhlmann and P. Muralt, *Adv. Mater.*, 2008, **20**, 3090.

3   F. Rubio-Marcos, A. D. Campo, R. Lopez-Juarez, J. J. Romeroa and J. F. Fernandez, *J. Mater. Chem.*, 2012, **22**, 9714.

4   Q. M. Zhang, H. Wang, N. Kim and L. E. Cross, *J. Appl. Phys.*, 1994, **75**, 454.

5   A. Pramanick, D. Damjanovic, J. C. Nino and J. L. Jones, *J. Am. Ceram. Soc.*, 2009, **92**, 2291.

6   R. E. Eitel, T. R. Shrout and C. A. Randall, *J. Appl. Phys.*, 2006, **99**, 124110.

7   J. G. Wu, D. Q. Xiao and J. G. Zhu, *J. Appl. Phys.*, 2009, **105**, 056107.

8   J.-F. Li, Z.-X. Zhu and F.-P. Lai, *J. Phys. Chem. C*, 2010, **114**, 17796.

9   F. Griggio, S. Jesse, A. Kumar, O. Ovchinnikov, H. Kim, T. N. Jackson, D. Damjanovic, S. V. Kalinin and S. Trolier-McKinstry, *Phys. Rev. Lett.*, 2012, **108**, 157604.

10 K. J. Choi, M. Biegalski, Y. L. Li, A. Sharan, J. Schubert, R. Uecker, P. Reiche, Y. B. Chen, X. Q. Pan, V. Gopalan, L.-Q. Chen, D. G. Schlom and C. B. Eom, *Science*, 2004, **306**, 1005.

11 Y. B. Chen, M. B. Katz, X. Q. Pan, C. M. Folkman, R. R. Das and C. B. Eom. *Appl. Phys. Lett.*, 2007, **91**, 031902.

12 L. Polla and L. F. Francis, *Annu. Rev. Mater. Sci.*, 1998, **28**, 563.

13 N. Izyumskaya, Y. I. Alivov, S. J. Cho, H. Morko, H. Lee and Y. S. Kang, *Crit. Rev. Solid. State*, 2007, **32**, 111.

14 N. A. Pertsev and A. Y. Emelyanov, *Appl. Phys. Lett.*, 1997, **71**, 3646.

15 Z.-X. Zhu and J.-F. Li, *Appl. Surf. Sci.*, 2010, **256**, 3880.

16 R. J. Zednik, A. Varatharajan, M. Oliver, N. Valanoor and P. C. McIntyre, *Adv. Funct. Mater.*, 2011, **21**, 3104.

17 J. Karthik, J. C. Agar, A. R. Damodaran and L. W. Martin, *Phys. Rev. Lett.*, 2012, **109**, 257602.

18 Y. K. Kim, H. Morioka, S. Okamoto, T. Watanabe, S. Yokoyama, A. Sumi and H. Funakubo, *Appl. Phys. Lett.*, 2005, **87**, 182907.

19 Q. Yu, J.-F. Li, W. Sun, F.-Y. Zhu, Y. M. Liu, Y. N. Chen, Z. J. Wang and J. Y. Li, *Appl. Phys. Lett.*, 2014, **104**, 012908.

20 M. Pereira, A. G. Peixoto and M. J. M. Gomes, *J. Eur. Ceram. Soc.*, 2001, **21**, 1353.

21 J. G. Wu, J. L. Zhu, D. Q. Xiao, J. G. Zhu, J. Z. Tan, Q. L. Zhang and Y. Y. Wang, *Appl. Surf. Sci.*, 2007, **253**, 6222.

22 W. Gong, J.-F. Li, X. C. Chu, Z. L. Gui and L. T. Li, *Appl. Phys. Lett.*, 2004, **85**, 3818.

23 Q. Yu, J.-F. Li, Z.-X. Zhu, Y. Xu and Q.-M. Wang, *J. Appl. Phys.*, 2012, **112**, 014102.

24 G. Binnig and C. F. Quate, *Phys. Rev. Lett.*, 1986, **56**, 930.

25 P. Güthner and K. Dransfeld, *Appl. Phys. Lett.*, 1992, **61**, 1137.

26 Y. M. Liu, Y. H. Zhang, M.-J. Chow, Q. N. Chen and J. Y. Li, *Phys. Rev. Lett.*, 2012, **108**, 078103.

27 B. J. Rodriguez, C. Callahan, S. V. Kalinin and R. Proksch, *Nanotechnology.*, 2007, **18**, 475504.

28 Z.-X. Zhu, J.-F. Li, Y. Y. Liu and J. Y. Li, *Acta. Mater.*, 2009, **57**, 4288.

29 Z.-X. Zhu, J.-F. Li, F.-P. Lai, Y. H. Zhen, Y.-H. Lin, C.-W. Nan, L. T. Li and J. Y. Li, *Appl. Phys. Lett.*, 2007, **91**, 222910.

30 J. Karthik, A. R. Damodaran and L. W. Martin, *Phys. Rev. Lett.*, 2012, **108**, 167601.

31 K. S. Lee, Y. K. Kim, S. Baik, J. Kim and I. S. Jung, *Appl. Phys. Lett.*, 2001, **79**, 2444.

32 H. Y. Liu, F. Zeng, Y. S. Lin, G. Y. Wang and F. Pan, *Appl. Phys. Lett.*, 2013, **102**, 181908.

33 S. Sun, Y. M. Wang, P. A. Fuierer and B. A. Tuttle, *Integr. Ferroelectr.*, 1999, **23**, 25.

34 S. Jesse, A. P. Baddorf and S. V. Kalinin, *Appl. Phys. Lett.*, 2006, **88**, 062908.

35 M. R. Soares, A. M. R. Senos and P. Q. Mantas, *J. Eur. Ceram. Soc.*, 2000, **20**, 321.

36 S. Utsugi, T. Fujisawa, Y. Ehara, T. Yamada, S. Yasui, M.-T. Chentir, H. Morioka, T. Iijima and H. Funakubo, *J. Ceram. Soc. Jpn.*, 2010, **118**, 627.

37 D. Su, Q. P. Meng, C. A. F. Vaz, M.-G. Han, Y. Segal, F. J. Walker, M. Sawicki, C. Broadbridge and C. H. Ahn, *Appl. Phys. Lett.*, 2011, **99**, 102902.

38 B. T. Liu, K. Maki, Y. So, V. Nagarajan, R. Ramesh, J. Lettieri, J. H. Haeni, D. G. Schlom, W. Tian, X. Q. Pan, F. J. Walker and R. A. McKee, *Appl. Phys. Lett.*, 2002, **80**, 4801.

39 K. S. Hwang, T. Manabe, T. Nagahama, I. Yamaguchi, T. Kumagai and S. Mizuta, *Thin. Solid. Films.*, 1999, **347**, 106.

6 | *J. Mater. Chem. C*, 2013, **00**, 1-3

This journal is © The Royal Society of Chemistry 2012